1056 J. Med. Chem. 2010, 53, 1056–1066
DOI: 10.1021/jm9012328

Journal of Medicinal Chemistry Article

# Optimization of a Pipemidic Acid Autotaxin Inhibitor

Adrienne B. Hoeglund,[†,‡] Heidi E. Bostic,[§] Angela L. Howard,[†,‡] Irene W. Wanjala,[†,‡] Michael D. Best,[§] Daniel L. Baker,*[,†] and Abby L. Parrill*[,†,‡]

[†]Department of Chemistry, and [‡]Computational Research on Materials Institute, The University of Memphis, Memphis, Tennessee 38152, and [§]Department of Chemistry, The University of Tennessee, Knoxville, Knoxville, Tennessee 37996

Received August 18, 2009

Autotaxin (ATX, NPP2) has recently been shown to be the lysophospholipase D responsible for synthesis of the bioactive lipid lysophosphatidic acid (LPA). LPA has a well-established role in cancer, and the production of LPA is consistent with the cancer-promoting actions of ATX. Increased ATX and LPA receptor expression have been found in numerous cancer cell types. The current study has combined ligand-based computational approaches (binary quantitative structure−activity relationship), medicinal chemistry, and experimental enzymatic assays to optimize a previously identified small molecule ATX inhibitor, H2L 7905958 (**1**). Seventy prospective analogs were analyzed via computational screening, from which 30 promising compounds were synthesized and screened to assess efficacy, potency, and mechanism of inhibition. This approach has identified four analogs as potent as or more potent than the lead. The most potent analog displayed an $IC_{50}$ of 900 nM with respect to ATX-mediated FS-3 hydrolysis with a $K_i$ of 700 nM, making this compound approximately 3-fold more potent than the previously described lead.

## Introduction

Autotaxin (ATX, NPP2)[a] was originally identified as an autocrine motility factor in the conditioned media of A2058 melanoma cells.[1] Subsequently, ATX was shown to be the lysophospholipase D enzyme responsible for synthesis of the bioactive lipid lysophosphatidic acid (LPA) *in vivo*.[2,3] Recent work has shown that ATX plays critical roles in normal human development[4−7] and disease. ATX has been linked to cancer progression,[8−20] multiple sclerosis,[21] obesity,[22−26] diabetes,[22] Alzheimer's disease,[27] and chronic pain[28−30] through the production of LPA. Specific, potent inhibitors of ATX are therefore desirable as novel therapeutic leads.

Examples of metal chelators, lipid analogs, and nonlipid small molecules have all been identified as autotaxin inhibitors. Metal chelators such as EDTA,[31] phenanthroline,[31] and L-histidine[32] have been shown to inhibit ATX activity, presumably via interactions with active site divalent metal ions required for function. Lipid analogs represent the largest group of reported ATX inhibitors (see Figure 1 for structures). LPA and the related bioactive lipid sphingosine 1-phosphate (S1P) were previously shown to function as feedback inhibitors of ATX.[33] This discovery led to the analysis of several LPA and S1P analogs as ATX inhibitors. Reported LPA analogs include fatty alcohol phosphates,[34] Darmstoff analogs,[35] cyclic phosphatidic acid analogs,[36] and phosphonates.[37−39] One reported S1P analog, FTY720-phosphate (**32**), has also been examined as an ATX inhibitor.[40] While many of these lipid analogs are potent ATX inhibitors, they lack many characteristics seen in 90% of orally bioavailable drugs,[41,42] and collectively they lack significant structural diversity. Finally, the third category of reported ATX inhibitors consists of nonlipid small molecules that collectively extend structural diversity and in general possess physicochemical characteristics more closely related to orally bioavailable drugs. Our group was the first to report the identification of small molecule ATX inhibitors using virtual screening (binary QSAR and homology modeling) approaches.[43] The most efficacious structures identified from that work are shown in Figure 2A.[43] H2L 7905958 (**1**) was the most efficacious compound from that initial single concentration screen (at 10 $\mu$M, compound **1** fully inhibited ATX-catalyzed hydrolysis of 1 $\mu$M FS-3).[43] Recently, Saunders and colleagues identified additional small molecule inhibitors of ATX (Figure 2B,C) as metastasis blockers.[44] One compound showed essentially 100% inhibition of melanoma metastasis at micromolar concentrations.[44]

In this study, we investigated the structure−activity relationships of our most efficacious previously published small molecule ATX inhibitor, compound **1** (Figure 3A, ChemBridge, San Diego, CA).[43] Using a combination of binary QSAR modeling and synthetic optimization, we prepared 30 analogs of compound **1** and subjected them to pharmacological characterization using the FRET-based, synthetic ATX substrate FS-3.[45] Four of these 30 compounds exhibited $IC_{50}$ values less than or equal to the lead. Despite their structural similarity, three of four reversible classes of inhibition (competitive, mixed-mode, and noncompetitive) were observed within this series. Inhibitors in these three classes share the ability to bind to the enzyme in the absence of substrate, reflected by $K_i$. Mixed-mode and noncompetitive inhibitors additionally have the ability to bind to the enzyme−substrate complex, reflected by $K_i'$. The $K_i$ values, due to their independence of substrate identity, suggest that the inhibition observed will

*Corresponding Authors: Phone: 901-678-2638 (ALP), 901-678-4178 (DLB). Fax: 901-678-3447. E-mail addresses: aparrill@memphis.edu, dlbaker@memphis.edu.

 Published on Web 12/30/2009 

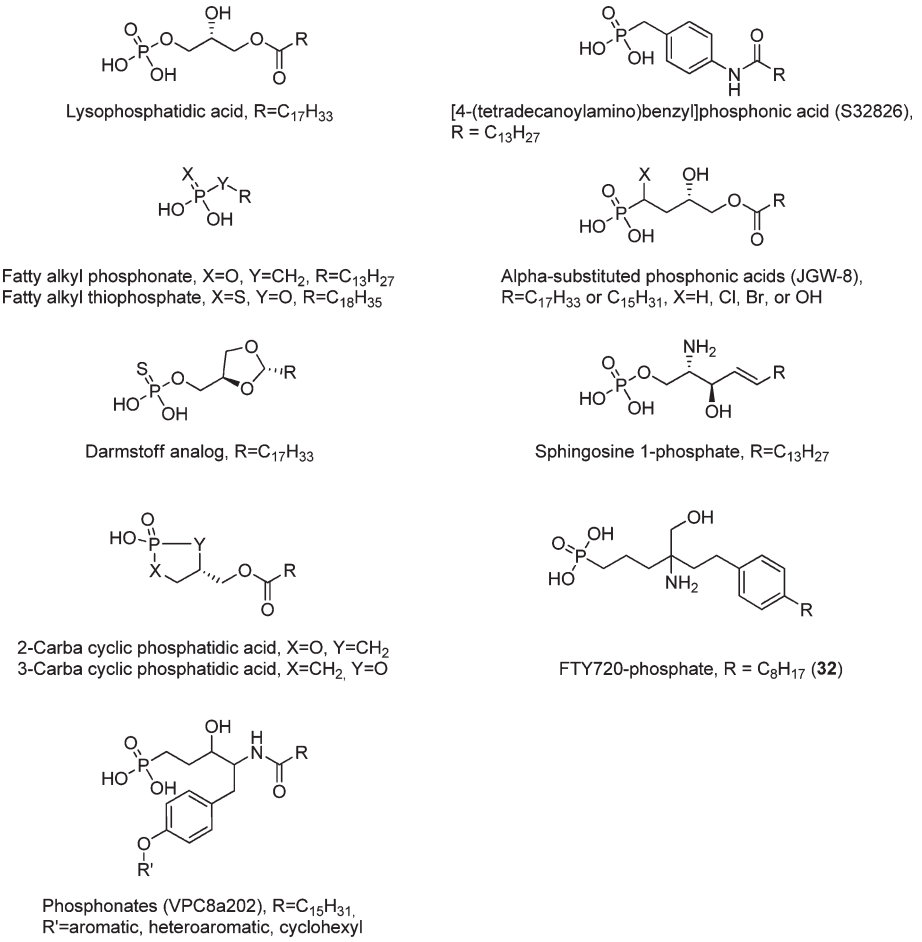


**Figure 1.** Structures of published lipid-like ATX inhibitors.[33−38,40,54,55]

transfer to inhibition of ATX-catalyzed inhibition of its natural substrate, lysophosphatidylcholine (LPC).

## Results

In 2008, we identified compound **1** (Figure 3A) as a potent ATX inhibitor.[43] This compound (10 $\mu$M) completely blocked ATX-mediated hydrolysis of the synthetic FRET reagent FS-3 (1 $\mu$M). Following this initial report, we determined that compound **1** inhibited ATX with an $IC_{50}$ of 1.6 ± 0.4 $\mu$M (Figure 3B). Simultaneous nonlinear regression of the inhibition kinetics data shown in Figure 3C, using an average $K_m$ value of 3.7 ± 1.9 $\mu$M ($n$ = 22) produced the best fit to a competitive inhibition mechanism, with a $K_i$ of 1.9 $\mu$M. With a low micromolar inhibitor lead in hand, we next sought a convenient diversification strategy to generate structure−activity relationship (SAR) data in hopes of better understanding ATX inhibitor recognition and identifying more potent analogs. Here, the derivatization of pipemidic acid with commercially available isothiocyanate building blocks was identified as a facile route to a range of analogs of compound **1** bearing various substituents on the phenylthiourea motif (Figure 4).

Using this diversification approach, 70 proposed synthetic analogs of compound **1** (Figure 5 and Supplemental Figure 1, Supporting Information) were evaluated and prioritized using a general binary QSAR model[43] (model A) before they were synthesized. This general model was trained on a diverse set of compounds (298 total compounds) including both lipid and nonlipid analogs. Of these, 238 lacked ATX inhibition (inactive) and 60 showed ATX inhibition ≥50% at 10 $\mu$M (active). An initial set of nine compounds, containing either ortho or para substituents (Figure 5B), was synthesized based on these predicted activities. Experimental assays using a single dose of 10 $\mu$M demonstrated that all nine compounds were less efficacious than the parent (Table 1) and only two showed ≥50% inhibition. This data suggests that model A, based on a diverse training set, was unable to accurately predict activity within this narrow structural series.

A more class-specific binary QSAR model (model B) was constructed for use in lead optimization. This refined model was trained on 248 compounds of which 204 were inactive and 44 were active. The training set for model B differed from that used for model A in three ways. First, it lacked lipid-like ATX inhibitors (Figure 2). Second, the nine initial analogs utilized as the test set for model A were added (Figure 5B). Third, it was augmented with an additional 12 analogs of compound **1** (Figure 5C) synthesized to better represent diversity within this SAR series. The total internal accuracy of the model was 86%, with 59% accuracy for actives and 91% accuracy for inactives.

The predictive accuracy of models A and B were examined using an additional nine compound test set (Figure 5D). Both models predicted four of the nine compounds (with only one of the four being the same analog) to be active. Screening results showed that model A was 67% accurate in predicting active compounds and 33% accurate on both inactive compounds and total accuracy. These predictions fell short of expectations based on the training set results. Overall, model

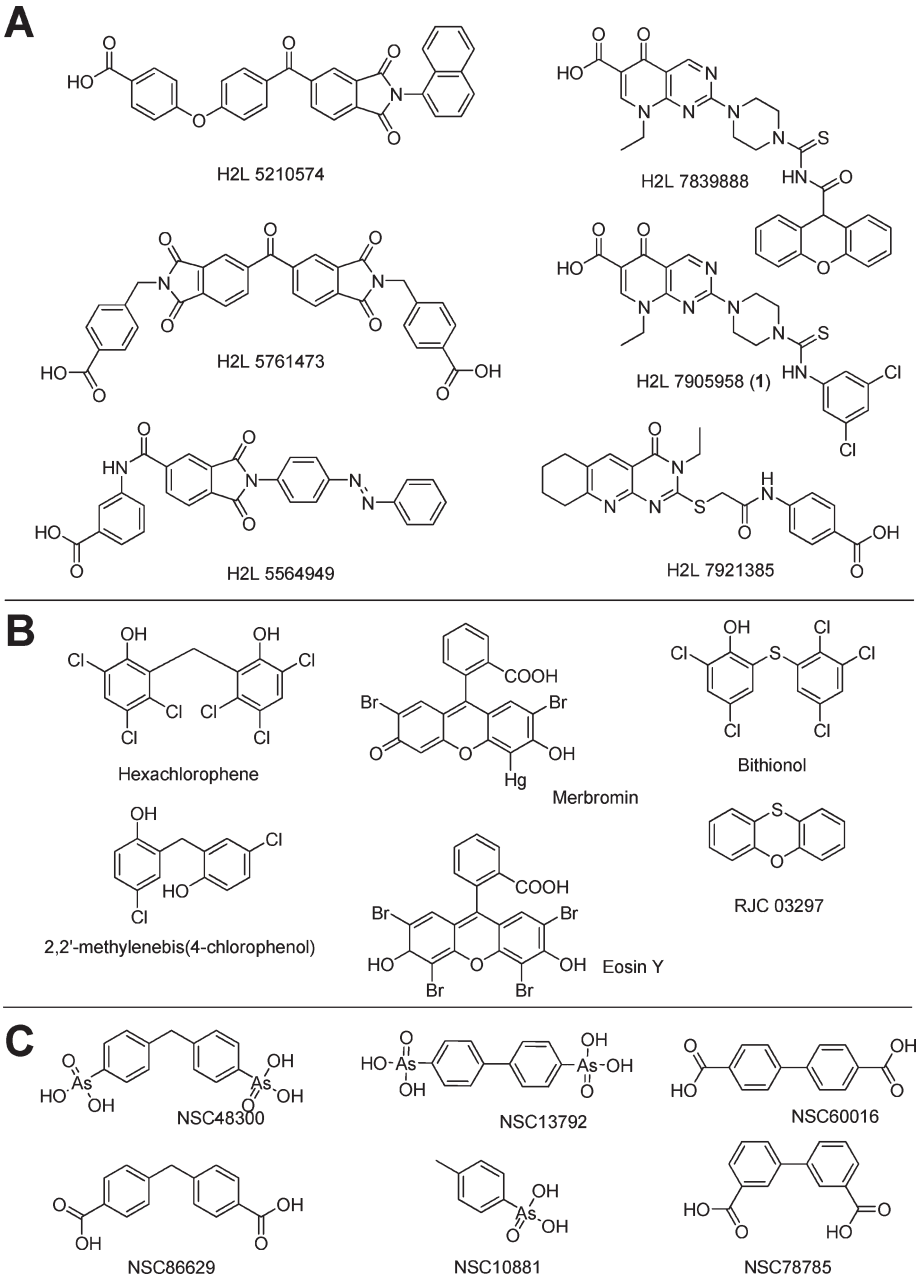


**Figure 2.** Structures of published nonlipid ATX inhibitors: (A) H2L compounds;[43] (B) structures of hexachlorophene, merbromine, bithionol, and their analogs;[44] (C) ATX inhibitors identified from the NCI database.[44]

A failed to be predictive for this closely related SAR series. Model B was shown to be 75% accurate in predicting active compounds and 40% accurate on inactive compounds, with a total accuracy of 56%. These predictions were consistent with expectations based on the training set results.

Of the original 70 proposed analogs (Figure 5 and Supplemental Figure S1, Supporting Information), 30 compounds were synthesized (Figure 5) based on computational results. These analogs provided diverse substituent types and substitution patterns (Table 1) to serve as a training set suitable for specific activity prediction within this SAR series. The resulting analogs were examined for their ability to inhibit ATX-mediated hydrolysis of FS-3 at 10 $\mu$M. Likewise, each analog was tested in the presence of carboxyfluorescein (the product of ATX-mediated hydrolysis of FS-3) to identify false positive or negative results. None of the analogs tested significantly altered carboxyfluorescein fluorescence. Compounds containing meta substituents demonstrated ATX inhibition in the range of 60−100%. Compound **11** (Figure 5C), with a trifluoromethyl group in the meta position, yielded 100% inhibition. A comparative assay of the 15 analogs showing $>50\%$ inhibition was performed against both CCM and purified ATX (8.3 nM enzyme concentration) to confirm that relative potencies were independent of enzyme source. The results showed that the potency rank of the inhibitors was unchanged and that the results were within $\pm 5\%$ (data not shown).

The selectivities of ATX inhibitors **3**, **7**, **11**, **13**, **14**, **18**, **19**, **20**, **22**, **23**, **25**, **27**, **28**, **29**, and **31**, all of which inhibited ATX-mediated hydrolysis of FS-3 by $\geq 50\%$ at single doses of 10 $\mu$M, were examined against NPP6 and NPP7, the only other known lipid preferring NPP isoforms. None of the 15 compounds effected the activity of NPP6 or NPP7 (Supplemental Figure S2, Supporting Information). Likewise, each

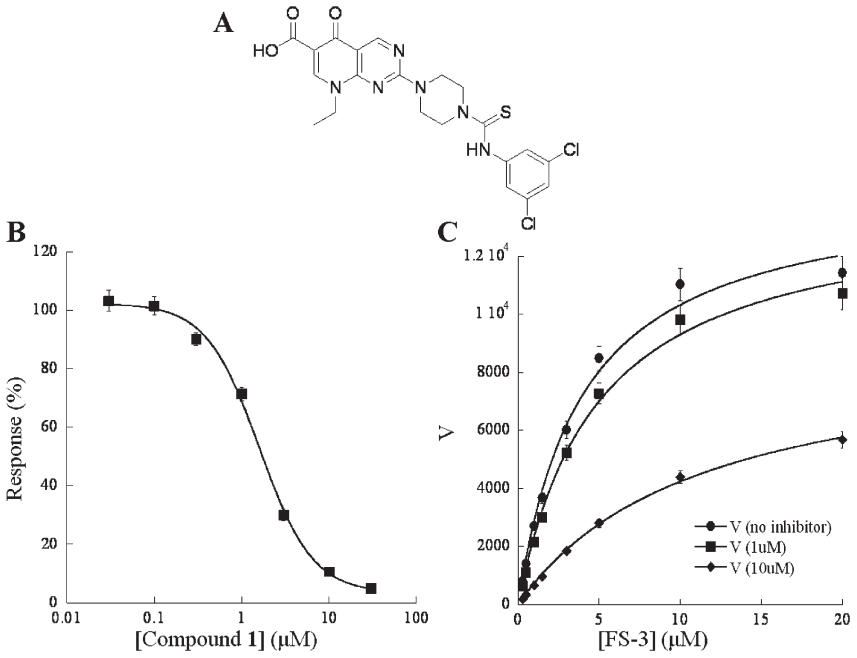


**Figure 3.** Structure (panel A) and pharmacology of **1**: (B) dose−response determined using 1 $\mu$M FS-3 gives $IC_{50}$ = 1.6 $\mu$M ($IC_{50}$ values were within ±3%, determination was based on average of two runs); (C) inhibitor effect on kinetics of FS-3 hydrolysis by ATX best fits competitive inhibition ($K_i$ = 1900 nM).

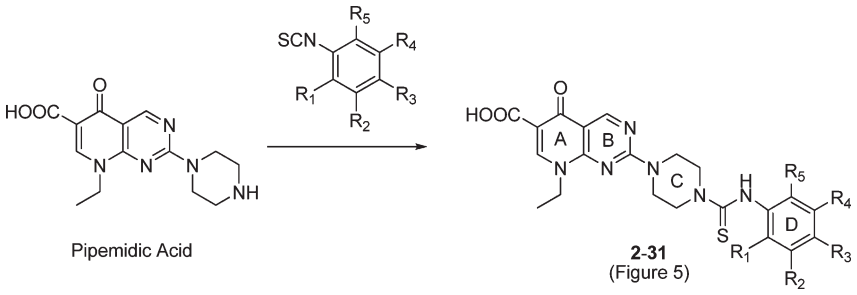


**Figure 4.** Synthetic scheme for the synthesis of analogs of **1** using commercially available pipemidic acid and isothiocyanates.

analog was tested in the presence of *p*-nitrophenol (the product of ATX-mediated hydrolysis of *p*-nitrophenylphosphorylcholine (pNPPC)) to eliminate the chance of false positive or false negative results. None of the analogs tested had a significant effect on the *p*-nitrophenol absorbance.

Dose−response curves were determined for all 15 analogs that inhibited ATX-mediated hydrolysis of FS-3 by ≥50% at 10 $\mu$M. $IC_{50}$ values in a range of 900 nM to 17.7 $\mu$M were observed (Figure 6 and Table 1). Compounds demonstrating an $IC_{50}$ less than 15 $\mu$M were further examined to determine their mechanism of inhibition by simultaneous nonlinear regression of kinetic data to competitive, uncompetitive, mixed, and noncompetitive kinetic inhibition equations. The mechanism giving the lowest average percent residual errors was selected. $K_i$ (competitive, mixed, or noncompetitive) and $K_i'$ (mixed, noncompetitive, or uncompetitive) values, representing affinity for the enzyme or the enzyme−substrate complex, respectively, were obtained from the simultaneous nonlinear regression (Table 1). None of the inhibitors proved to act by uncompetitive inhibition; therefore each was capable of binding to the enzyme in the absence of substrate. Compounds **7**, **11**, **13**, **18**, **22**, and **28** were competitive ATX inhibitors with $K_i$ values ranging from 700 to 7100 nM. Analog **11** has 3 times greater affinity for the enzyme than the lead. Compounds **3**, **14**, **20**, and **29** were mixed-mode ATX inhibitors with $K_i$ values ranging from 2.6 to 13.2 $\mu$M. These compounds showed reduced affinity for the enzyme−substrate complex compared with their affinity for the enzyme as reflected in higher $K_i'$ values ranging from 11.0 to 47.3 $\mu$M. Compound **31** showed noncompetitive inhibition with a $K_i/K_i'$ value of 13.2 $\mu$M. The mixed and noncompetitive inhibitors, **3**, **14**, **20**, **29**, and **31**, have the ability to bind to the enzyme−substrate complex as well as the enzyme. The noncompetitive inhibitor, **31**, binds with identical affinity to both the enzyme and enzyme−substrate complex.

Table 2 provides a summary of single-dose data that provides SAR insights. These data clearly demonstrate that inhibition is greatest when substituents appear at the meta position, followed by para with the weakest inhibition at the ortho position. This trend is consistent for all substituents examined.

## Discussion

Interest in ATX as a therapeutic target is growing due to its association with a number of human diseases including various cancers.[8−30] This interest is reflected in a rising number of reported ATX inhibitors with potencies in the nanomolar range (Figure 1). Carbacyclic analogs of cyclic phosphatidic acid (3ccPA) were demonstrated to be potent

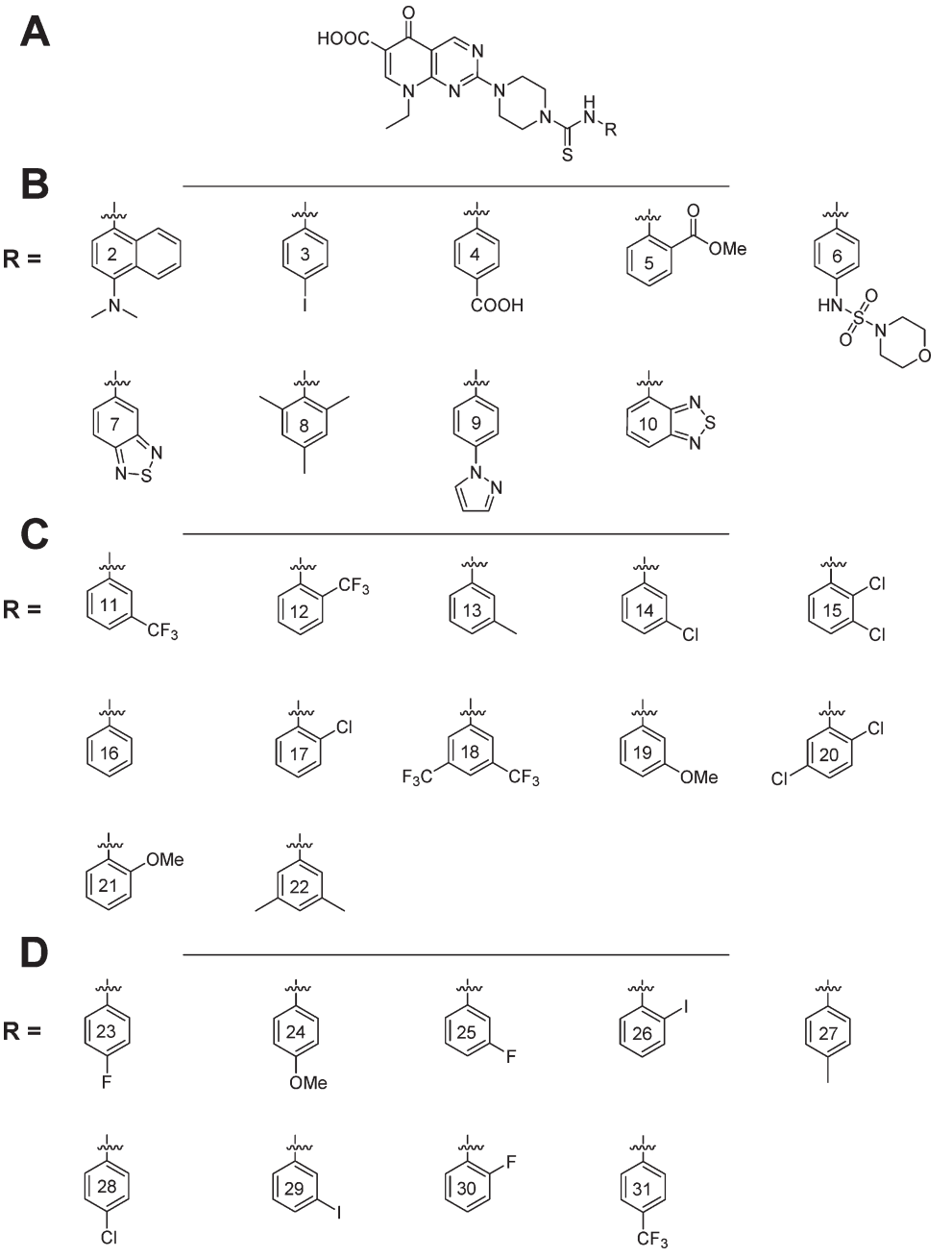


**Figure 5.** Structures of the 30 synthetic analogs of compound **1**: (A) common structural core where R represents the components seen in panels B−D; (B) compounds synthesized based on initial predictions using binary QSAR model A; (C) compounds synthesized to augment binary QSAR training set for model B; (D) compounds synthesized to serve as the binary QSAR test set for model B.

inhibitors of ATX that failed to activate LPA GPCR.[36] ATX inhibition by 3ccPA translated to reduced cancer cell invasion *in vitro* and reduction of cancer cell metastasis *in vivo*.[36] The LPA analog, fluoromethylene phosphonate, was shown to be an effective ATX inhibitor, while also a modest $LPA_{1/3}$ antagonist.[39] Darmstoff analogs of LPA were examined for their potential as LPA GPCR agonists and were shown to inhibit ATX in the nanomolar range.[35] Compound **32**, a phosphorylated immunomodulator, was shown to inhibit ATX-mediated production of LPA *in vivo*.[40] Another lipid phosphonate analog, S32826 (Figure 1), was reported to have potency in the nanomolar range.[38] $\beta$-hydroxy and $\beta$-keto phosphonate derivatives of LPA were studied as potential ATX inhibitors. VPC8a202 (Figure 1), a $\beta$-hydroxy derivative, was identified as a potent ATX inhibitor.[37] A common structural theme among these potent ATX inhibitors is their overall lipid nature, with polar headgroups and nonpolar tails.

The development of highly potent nonlipid inhibitors has been hampered by limited information about the three-dimensional structure of ATX. Nevertheless, several groups have reported nonlipid inhibitors,[44,46] albeit with much poorer potencies than the current lipid-like inhibitors. The current work focused on elaborating the SAR for compound **1**, a previously identified, nonlipid ATX inhibitor, in our efforts to better understand the structure of the binding pocket, as well as to improve the potency of a known nonlipid inhibitor.[43] For this study, 70 potential analogs of **1** were designed based on a one-step synthetic scheme benefiting from commercially available pipemidic acid and substituted phenyl isothiocyanates. In total, 30 compounds were synthesized and evaluated.

**Table 1.** SAR Elaboration and Optimization of Lead Compound **1**[a]

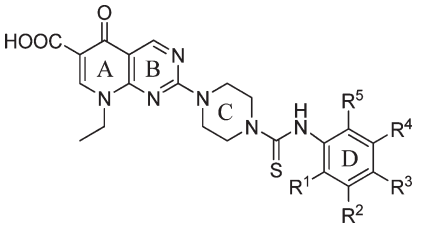


| substitution on D ring | % response at 10 $\mu$M (FS-3) | $IC_{50}$ ($\mu$M) | inhibition mechanism | $K_i$ ($\mu$M) | $K_i'$ ($\mu$M) |
|---|---|---|---|---|---|
| lead - dichloro ($R^2$, $R^4$) (**1**) | 0.0 ± 4.0 | 1.6 ± 0.4 | competitive | 1.9 | |
| *trifluoromethyl* (*meta - R*$^2$) (***11***) | *0.3 ± 0.6* | *0.9 ± 0.3* | *competitive* | *0.70* | |
| **dichloro (R$^1$, R$^4$) (20)** | **5.4 ± 0.4** | **1.3 ± 0.2** | **mixed** | **3.4** | **22.0** |
| **iodo (meta - R$^2$) (29)** | **8.6 ± 0.9** | **1.6** | **mixed** | **7.4** | **11.0** |
| chloro (meta - $R^2$) (**14**) | 9.7 ± 0.9 | 2.5 ± 0.2 | mixed | 2.6 | 47.3 |
| thiadiazole ($R^2$,$R^3$) (**7**) | 28.6 ± 2.0 | 12.1 ± 2.4 | competitive | 7.1 | |
| dimethyl ($R^2$, $R^4$) (**22**) | 30.4 ± 1.3 | 9.0 | competitive | 4.2 | |
| iodo (para - $R^3$) (**3**) | 32.7 ± 1.3 | 5.6 ± 0.2 | mixed | 13.2 | 34.1 |
| ditrifluoromethyl ($R^2$, $R^4$) (**18**) | 34.1 ± 3.0 | 4.4 ± 1.5 | competitive | 4.0 | |
| **trifluoromethyl (para - R$^3$) (31)** | **36.2 ± 0.9** | **1.5 ± 0.1** | **noncompetitive** | **13.2** | **13.2** |
| fluoro (meta - $R^2$) (**25**) | 40.5 ± 1.0 | 16.1 ± 4.5 | | | |
| methoxy (meta - $R^2$) (**19**) | 40.9 ± 1.3 | 17.7 ± 0.3 | | | |
| methyl (meta - $R^2$) (**13**) | 41.9 ± 0.8 | 13.5 ± 1.3 | competitive | 4.5 | |
| chloro (para - $R^3$) (**28**) | 42.4 ± 0.9 | 10.7 | competitive | 5.7 | |
| fluoro (para - $R^3$) (**23**) | 48.9 ± 1.1 | 17.7 | | | |
| methyl (para − $R^3$) (**27**) | 49.9 ± 1.5 | 16.1 ± 4 | | | |
| *o*-methyl ester (**5**) | 51.2 ± 1.3 | | | | |
| trimethyl ($R^1$, $R^3$, $R^5$) (**8**) | 53.5 ± 1.6 | | | | |
| H (**16**) | 56.4 ± 1.0 | | | | |
| 4-dimethylaminonapthyl (**2**) | 59.9 ± 1.5 | | | | |
| thiadiazole ($R^1$,$R^2$) (**10**) | 63.2 ± 2.8 | | | | |
| sulfonylmorpholine (para − $R^3$) (**6**) | 64.1 ± 2.8 | | | | |
| iodo (ortho − $R^1$) (**26**) | 68.4 ± 1.3 | | | | |
| pyrazole (para − $R^3$) (**9**) | 68.6 ± 1.1 | | | | |
| dichloro ($R^1$, $R^2$) (**15**) | 72.3 ± 0.4 | | | | |
| *p*-carboxyl (**4**) | 72.7 ± 2.2 | | | | |
| fluoro (ortho − $R^1$) (**30**) | 77.3 ± 1.6 | | | | |
| methoxy (para − $R^3$) (**24**) | 79.7 ± 0.9 | | | | |
| chloro (ortho - $R^1$) (**17**) | 83.5 ± 8.2 | | | | |
| Methoxy (ortho − $R^1$) (**21**) | 97.6 ± 1.8 | | | | |
| trifluoromethyl (ortho − $R^1$) (**12**) | 100.8 ± 1.9 | | | | |

[a] Compounds showing equal or improved $IC_{50}$ (bold) or $K_i$ (italic) values over the lead are emphasized. Values shown in parentheses refer to the compound numbers (Figure 5). Errors where indicated are standard deviations of at least three independent experiments. $IC_{50}$ values lacking standard deviations are averages of two independent experiments that were less than 3% different in value.

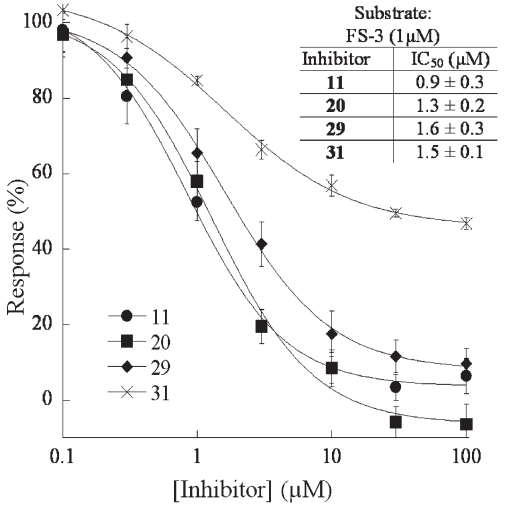


**Figure 6.** Dose−response plots of the four compounds (**11**, **20**, **29**, and **31**) equivalent to or more potent than the lead compound.

**Table 2.** Single-Dose Response Comparison by Aromatic Substituent and Position[a]

| | meta-$R^2$ | para-$R^3$ | ortho-$R^1$ |
|---|---|---|---|
| trifluoromethyl | 0.3 ± 0.6 (**11**) | 36.2 ± 0.9 (**31**) | 100.8 ± 1.9 (**12**) |
| iodo | 8.6 ± 0.9 (**29**) | 32.7 ± 1.3 (**3**) | 68.4 ± 1.3 (**26**) |
| chloro | 9.7 ± 0.9 (**14**) | 42.4 ± 0.9 (**28**) | 83.5 ± 8.2 (**17**) |
| fluoro | 40.5 ± 1.0 (**25**) | 48.9 ± 1.1 (**23**) | 77.3 ± 1.6 (**30**) |
| methoxy | 40.9 ± 1.3 (**19**) | 79.7 ± 0.9 (**24**) | 97.6 ± 1.8 (**21**) |

[a] Values shown in parentheses refer to the compound numbers (Figure 5).

Table 2 summarizes two important trends that we observed with these analogs. First, inhibition improves going from ortho to para to meta substituent positions regardless of the substituent type. This suggests that meta substituents are preferred for steric or conformational, rather than electronic reasons. Second, in the meta-substituted series inhibition improves in the order of methoxy, fluoro, chloro, iodo, and trifluoromethyl. This order reflects neither size nor electronic trends among these substituents. Four compounds (**11**, **20**, **29**,

and **31**) were at least as potent as the lead compound (**1**). A single meta-trifluoromethyl (**11**, $K_i = 0.70\ \mu M$) was preferred over two (**18**, $K_i = 4.0\ \mu M$), Table 1. In fact, *meta*-trifluoromethyl (**11**) showed three times higher affinity for the enzyme than the lead compound, while the disubstituted trifluoromethyl (**18**) exhibited 2-fold less enzyme affinity than the lead. This suggests that one of the two meta substituents is located in a substantially larger pocket than the other.

These SAR trends inform the development of computational tools aimed toward the identification and optimization of ATX inhibitors such as our previously reported binary QSAR model.[43] An updated binary QSAR model was developed for this work by the addition of more nonlipid and lipid-like compounds (published since our initial report) in an attempt to improve the accuracy of prediction (model A). We found this model unable to accurately predict activity differences due to the very small structural changes examined in this work. This is in large part due to its originally intended use to screen diverse chemical collections for leads with varied structures. To circumvent this issue, a more class-specific model for lead optimization was designed (model B). When predicted against the training set, model B showed an 11% improvement over model A in predicting active compounds, 18% in inactive prediction, and an overall 41% improvement in total prediction. Further improvements are expected, however, when training sets can be segregated on the basis of mechanism of inhibition.

Previously published research defines inhibition mechanisms for a relatively small proportion of the known inhibitors. Inhibitors with reported mechanism of inhibition include L-histidine,[32] LPA and S1P,[33] **32**,[40] and nonlipid small molecules.[44] L-Histidine demonstrates noncompetitive inhibition. LPA and S1P demonstrated mixed-mode inhibition with LPA having a $K_i$ of $\sim 0.1\ \mu M$.[33] van Meeteren and colleagues also reported that **32** inhibited ATX in the low micromolar range by a competitive mechanism with a $K_i$ of $0.2\ \mu M$.[40] Finally, Saunders and colleagues demonstrated nanomolar potency for a nonlipid small molecule competitive ATX inhibitor (Figure 2C).[44] Within the series of analogs synthesized here, we observed competitive, mixed mode, and noncompetitive inhibition mechanisms. All inhibitors tested showed affinity for the enzyme in the absence of substrate, so the results suggest that these inhibitors will be effective in assays reflecting inhibition of LPC hydrolysis. Future computational tools to be developed using the $K_i$ values reported here include traditional QSAR models, which not only will be able to predict likelihood that candidates will exhibit inhibition better than a threshold value but will actually be able to predict the affinity for the enzyme.

Inhibitor specificity in the NPP family has previously not been examined. Three members of the NPP enzyme family, NPP2 (ATX), NPP6, and NPP7, share the ability to hydrolyze lysophospholipids[47] and therefore might be expected to have some overlap in their recognition of inhibitors. Supplemental Figure 2, Supporting Information, illustrates the selectivity of compounds inhibiting at least 50% of ATX activity (Table 1) over NPP6 and NPP7. These analogs clearly do not inhibit NPP6 or NPP7 at a single $10\ \mu M$ dose. These inhibitors are therefore selective for ATX among the NPP isoforms with demonstrated preference for phospholipid substrates.

## Conclusions

Thirty out of 70 potential analogs of compound **1** were synthesized based on binary QSAR predictions. These 30 analogs were characterized as ATX inhibitors using single-dose screening, analysis of selectivity against other lipid preferring NPP isoforms, dose−response determinations, and mechanism of inhibition analysis ($K_i$ determination). The 15 analogs that inhibited ATX activity $\geq 50\%$ at $10\ \mu M$ were shown to be ATX selective. Eight analogs exhibited $IC_{50}$ for ATX-mediated FS-3 hydrolysis less than $10\ \mu M$. Six of these analogs exhibited competitive ATX inhibition with $K_i$ values ranging from 700 nM to $7.1\ \mu M$. The best of these compounds has a potency ($K_i = 700$ nM) approaching that reported for some of the most active published nonlipid ATX inhibitors.

## Experimental Section

**Binary QSAR Model Development.** Binary QSAR model A was developed from the expansion of model 1 in ref 43. Model A was trained on a diverse set of 298 compounds (60 active and 238 inactive) consisting of both lipid-like analogs and nonlipids. Model B was trained on 248 compounds of which 204 were inactive and 44 were active. This training set did not contain the lipid-like compounds present in model A. The compounds in models A and B were not corrected for explicit hydrogen atoms or charges on ionizable groups. Compounds were classified active if at least 50% inhibition was observed at a concentration of $10\ \mu M$. Over 220 structural descriptors, available in the current version of the MOE software, were calculated for each compound (both models). Descriptors that were dependent upon the orientation of the compound in a coordinate system and those involving semiempirical quantum mechanics were not included in the analysis. The individual descriptors were reduced to a set of orthogonal principal components. The binary models were fitted using seven principal components.

**Determination of ATX Inhibition.** ATX inhibition was determined using the synthetic FRET-based substrate FS-3 (Echelon Biosciences, Inc., Salt Lake City, UT). Concentrated ($\sim 10\times$) conditioned medium (CCM) from MDA-MB-435 cells was used as the source of ATX. The final volume ($60\ \mu L$) included $20\ \mu L$ of CCM, $20\ \mu L$ of inhibitor ($10\ \mu M$ for single point experiments or 30 nM to $30\ \mu M$ for dose−response experiments, including 1% DMSO) in assay buffer (1 mM each $CaCl_2$ and $MgCl_2$, 5 mM KCl, 140 mM NaCl, 50 mM Tris, pH 8.0), and $20\ \mu L$ of FS-3, $1\ \mu M$ in assay buffer containing charcoal-stripped,[48] fatty acid free BSA ($30\ \mu M$) (Sigma Aldrich, St. Louis, MO). All assays were performed in 96-well, half-area plates (Corning Inc., Lowell, MA) at 37 °C with data collected at 2 min intervals using a Synergy2 fluorescence plate reader (BioTek, Winooski, VT). Fluorescence resulting from the hydrolysis of FS-3 was monitored using excitation at 485 nm and emission at 528 nm.[45] Results were derived from the 1 h time point, where all fluorescence changes were linear as a function of time. All readings were normalized to vehicle control after subtraction of fluorescence in the absence of CCM. Carboxyfluoroscein (Sigma-Aldrich, St. Louis, MO) in the absence of ATX was used as an analog of the FS-3 hydrolytic fluorophore in experiments to confirm that the analogs did not provide false positive (signal quenching) or false negative (signal enhancing) results, respectively. Final volumes ($60\ \mu L$) consisted of $20\ \mu L$ of carboxyfluoroscein (200 nM) with $20\ \mu L$ of each analog ($10\ \mu M$), and $20\ \mu L$ of charcoal-stripped BSA ($30\ \mu M$) in assay buffer as described. Data were collected in a single point analysis using excitation at 485 nm and emission at 528 nm. Data are shown as the mean ± SD of at least three wells. All experiments were repeated at least twice, and representative results are shown.

**Mechanism of Inhibition.** ATX kinetics assays were performed using substrate concentrations from 300 nM to $20\ \mu M$ and three different concentrations of inhibitor (corresponding to 0, 0.5, and 2 times the $IC_{50}$ for each analog). Normalized fluorescence results were plotted as a function of time to determine initial

rates. These initial rates for the zero inhibitor concentration were plotted against the substrate concentration and a rectangular hyperbolic curve was fitted to the data using KaleidaGraph (version 4.03, Synergy Software, Reading, PA) to determine $K_m$. Data for all three inhibitor concentrations were simultaneously fitted in the Michealis−Menton equations for competitive, uncompetitive, mixed-mode, and noncompetitive inhibition (shown below) using simultaneous nonlinear regression for each model using WinNonLin 6.1 (Pharsight, Mountain View, CA). Mechanism of inhibition was assigned to the model giving the lowest averaged percent residuals. $K_i$ and $K_i'$ values represent compound affinity for free enzyme and the enzyme−substrate complex, respectively.

$$\text{For competitive inhibition}: \quad V_0 = \frac{V_{max}[S]}{\alpha K_m + [S]}, \quad \text{where} \quad \alpha = 1 + \frac{[I]}{K_i}$$

$$\text{For uncompetitive inhibition}: \quad V_0 = \frac{V_{max}[S]}{K_m + \alpha'[S]}, \text{where } \alpha' = 1 + \frac{[I]}{K_i'}$$

$$\text{For mixed-mode inhibition}: \quad V_0 = \frac{V_{max}[S]}{\alpha K_m + \alpha'[S]}$$

$$\text{For noncompetitive inhibition, } \alpha = \alpha', \text{ therefore}: \quad V_0 = \frac{V_{max}[S]}{\alpha(K_m + [S])}$$

**ATX Expression.** MDA-MB-435 cells were cultured at 37 °C under a humidified atmosphere containing 5% $CO_2$ in Dulbecco's modified Eagle medium (DMEM) (MediaTech, Herndon, VA) containing 100 U/mL penicillin, 100 μg/mL streptomycin (Hyclone, Logan, UT), 5% fetal bovine serum (FBS) (Hyclone, Logan, UT), and 2 mM L-glutamine (Hyclone, Logan, UT). Upon reaching 80−95% confluency, the cells were washed twice with sterile phosphate-buffered saline. Serum-free DMEM containing L-glutamine and antibiotics was then added to the cells. Conditioned media was collected after 36−48 h of incubation with serum-free DMEM. The media was concentrated, ∼10×, and buffer-exchanged into Tris (50 mM, pH 7.4) containing 20% ethylene glycol using 30 kDa molecular weight cutoff filters (Millipore, Beverly, MA) in an Amicon pressure cell (Millipore, Beverly, MA). Aliquots of 10× conditioned media were stored at 4 °C.

**Determination of NPP6 and NPP7 Inhibition.** Inhibitor selectivity was assayed using *p*-nitrophenylphosphoryl-choline (pNPPC) (Sigma-Aldrich, St. Louis, MO) as substrate for NPP6 and NPP7. The final volume (60 μL) included 20 μL of CM, NPP6, or CCM, NPP7, 20 μL of inhibitor (10 μM including 1% DMSO) in assay buffer, and 20 μL of pNPPC (10 mM for NPP6 or 1 μM for NPP7) in assay buffer. NPP6 assay buffer contained 500 mM NaCl, 0.05% Triton X-100, and 100 mM Tris-HCl (pH 9.0),[49] whereas NPP7 assay buffer consisted of 50 mM Tris HCl, pH 8.5, 150 mM NaCl, and 10 mM taurocholic acid.[50−53] However, unlike the published methods, EDTA was not added to the NPP7 assay buffer. All assays were performed in 96-well, half-area plates (Corning Inc., Lowell, MA) at 37 °C with data collected at 2 min intervals using a Synergy2 absorbance plate reader (BioTek, Winooski, VT). Results are shown at the 1 h time point, when all absorbance changes as a function of time were linear. Readings were normalized to vehicle control after subtraction of absorbance in the absence of CM or CCM. Data are shown as the mean ± SD of at least three wells. All experiments were repeated twice, and representative results are shown.

Assays were performed with CM or CCM from HEK293 cells transiently transfected with NPP6 and -7 expression plasmids, respectively. HEK293 cells were seeded in Dulbecco's modified Eagle's medium (DMEM) containing 10% fetal bovine serum, 100 U/mL penicillin, 100 μg/mL streptomycin (Hyclone, Logan, UT), and 2 mM L-glutamine. HEK293 cells were grown overnight at 37 °C under 5% $CO_2$ to 80% confluence. The cells were then transfected with human NPP6ex[49] or human NPP7ex[52,53] expression plasmids in the pcDNA3.1(+) mammalian vector in the presence of Polyfect transfection reagent (Hyclone, Logan, UT). Six hours after transfection, the culture medium was changed to serum-free DMEM containing L-glutamine, and cells were incubated for 48 h. Expressed protein was collected (NPP6 and NPP7) and concentrated, ∼10× (NPP7), using 10 kDa molecular weight cutoff filters (Millipore, Beverly, MA) in an Amicon pressure cell (Millipore, Beverly, MA).

**General Procedure for the Synthesis of Prospective Inhibitors Shown in Figure 4.** To a solution of pipemidic acid in *N*,*N*-dimethylformamide (1 mL) was added the corresponding substituted phenyl isothiocyanate. In some cases, triethylamine was added to speed the reaction, while in others, the addition of this base led to the formation of byproducts and was thus avoided. The mixture was then allowed to stir at room temperature under nitrogen overnight. The solvent was then removed *in vacuo*, and the residue was extracted twice with methylene chloride from aqueous saturated ammonium chloride. The organic layers were combined, dried with magnesium sulfate, filtered, and concentrated. The resulting crude product was then purified by flash chromatography on silica gel eluting with methanol in methylene chloride (0−20%) to yield the corresponding thiourea products. All synthetic compounds were determined to be >95% pure by HPLC.

**2-(4-{[(4-Dimethylaminonapthylphenyl)amino]carbonothioyl}-1-piperazinyl)-8-ethyl-5-oxo-5,8-dihydropyrido[2,3-*d*]pyrimidine-6-carboxylic Acid (2).** Pipemidic acid (25 mg, 0.0824 mmol), 4-dimethylamino-1-napthylisothiocyanate (18.8 mg, 0.0824 mmol), and triethylamine (23 μL, 0.165 mmol) were used. Purification on silica yielded **2** (23 mg, 53%). $^1$H NMR (300 MHz, $CDCl_3$) δ 9.29 (s, 1H), 8.63 (s, 1H), 8.32−8.24 (m, 1H), 8.02−7.93 (m, 1H), 7.62−7.46 (m, 3H), 7.02 (d, $J$ = 7.95 Hz, 1H), 4.29 (q, $J$ = 6.90 Hz, 2H), 4.16−3.85 (m, 8H), 2.90 (s, 6H), 1.45 (t, $J$ = 7.08 Hz, 3H) ppm.

**2-(4-{[(4-Iodophenyl)amino]carbonothioyl}-1-piperazinyl)-8-ethyl-5-oxo-5,8-dihydropyrido[2,3-*d*]pyrimidine-6-carboxylic Acid (3).** Pipemidic acid (25 mg, 0.0824 mmol), 4-iodophenyl isothiocyanate (21.5 mg, 0.0824 mmol), and triethylamine (23 μL, 0.165 mmol) were used. Purification on silica yielded **3** (36 mg, 77%). $^1$H NMR (300 MHz, $CDCl_3$) δ 9.32 (s, 1H), 8.66 (s, 1H), 7.66 (d, $J$ = 6.94 Hz, 1H), 7.37 (s, 1H), 7.27 (s, 1H), 7.00 (d, $J$ = 7.44 Hz, 1H), 4.33 (q, $J$ = 6.90 Hz, 2H), 4.21−3.99 (m, 8H), 1.49 (t, $J$ = 7.14 Hz, 3H) ppm.

**2-(4-{[(4-Carboxylphenyl)amino]carbonothioyl}-1-piperazinyl)-8-ethyl-5-oxo-5,8-dihydropyrido[2,3-*d*]pyrimidine-6-carboxylic Acid (4).** Pipemidic acid (25 mg, 0.0824 mmol), 4-isothiocyanatobenzoic acid (14.8 mg, 0.0824 mmol), and triethylamine (23 μL, 0.165 mmol) were used. Purification on silica yielded **4** (23 mg, 58%). $^1$H NMR (300 MHz, DMSO) δ 9.71 (s, 1H), 9.24 (s, 1H), 8.98 (s, 1H), 7.87 (d, $J$ = 8.53 Hz, 2H), 7.49 (d, $J$ = 8.43 Hz, 2H), 4.45−4.39 (m, 2H), 4.10−4.03 (m, 8H), 1.38 (t, $J$ = 6.94 Hz, 3H) ppm.

**2-(4-{[(2-Methylesterphenyl)amino]carbonothioyl}-1-piperazinyl)-8-ethyl-5-oxo-5,8-dihydropyrido[2,3-*d*]pyrimidine-6-carboxylic Acid (5).** Pipemidic acid (25 mg, 0.0824 mmol), methyl 2-isothiocyanatobenzoate (16 mg, 0.0824 mmol), and triethylamine (23 μL, 0.165 mmol) were used. Purification on silica yielded **5** (24 mg, 59%). $^1$H NMR (300 MHz, $CDCl_3$) δ 11.14 (s, 1H), 9.35 (d, $J$ = 3.14 Hz, 1H), 8.77 (d, $J$ = 7.80 Hz, 1H), 8.69 (d, $J$ = 2.99 Hz, 1H), 8.01 (d, $J$ = 6.95 Hz, 1H), 7.55 (t, $J$ = 7.72 Hz, 1H), 7.12 (t, $J$ = 7.99 Hz, 1H), 4.38−4.12 (m, 10H), 3.92 (s, 3H), 1.51 (m, 3H) ppm.

**2-(4-{[(4-Morpholinosulfonylphenyl)amino]carbonothioyl}-1-piperazinyl)-8-ethyl-5-oxo-5,8-dihydropyrido[2,3-*d*]pyrimidine-6-carboxylic Acid (6).** Pipemidic acid (14.2 mg, 0.0468 mmol), 4-(morpholinosulfonyl)phenyl isothiocyanate (14 mg, 0.0468 mmol), and triethylamine (13 μL, 0.0935 mmol) were used. Purification on silica yielded **6** (24 mg, 85%). $^1$H NMR (300 MHz, $CDCl_3$) δ 9.28 (s, 1H), 8.65 (s, 1H), 8.09 (s, 1H), 7.64 (d, $J$ = 8.71 Hz, 2H), 7.51 (d, $J$ = 8.61 Hz, 2H), 4.43−4.01 (m, 10H), 3.80−3.70 (m, 4H), 3.04−2.98 (m, 4H), 1.49 (t, $J$ = 7.17 Hz, 3H) ppm.

**2-(4-{[(3-Benzothiadiazolphenyl)amino]carbonothioyl}-1-piperazinyl)-8-ethyl-5-oxo-5,8-dihydropyrido[2,3-*d*]pyrimidine-6-carboxylic Acid (7).** Pipemidic acid (25 mg, 0.0824 mmol),

2,1,3-benzothiadiazol-5-yl isothiocyanate (15.8 mg, 0.0824 mmol), and triethylamine (23 μL, 0.165 mmol) were used. Purification on silica yielded **7** (24 mg, 58%). $^1$H NMR (300 MHz, DMSO) δ 9.26 (s, 1H), 8.98 (s, 1H), 7.98−7.82 (m, 3H), 4.51−4.33 (m, 2H), 4.24−3.99 (m, 8H), 1.42−1.32 (m, 3H) ppm.

**2-(4-{[(2,4,6-Mesitylphenyl)amino]carbonothioyl}-1-piperazinyl)-8-ethyl-5-oxo-5,8-dihydropyrido[2,3-*d*]pyrimidine-6-carboxylic Acid (8).** Pipemidic acid (25 mg, 0.0824 mmol), mesityl isothiocyanate (14.6 mg, 0.0824 mmol), and triethylamine (23 μL, 0.165 mmol) were used. Purification on silica yielded **8** (36.6 mg, 92%). $^1$H NMR (300 MHz, $CDCl_3$) δ 9.32 (s, 1H), 8.64 (s, 1H), 7.05 (s, 1H), 6.92 (s, 2H), 4.41−3.93 (m, 10H), 2.28 (s, 3H), 2.23 (s, 6H), 1.50 (t, $J$ = 6.96 Hz, 3H) ppm.

**2-(4-{[(4-pyrazolephenyl)amino]carbonothioyl}-1-piperazinyl)-8-ethyl-5-oxo-5,8-dihydropyrido[2,3-*d*]pyrimidine-6-carboxylic Acid (9).** Pipemidic acid (27 mg, 0.0894 mmol) and 4-(1*H*-pyrazol-1-yl)phenyl isothiocyanate (15 mg, 0.0745 mmol) were used. Purification on silica yielded **9** (35.5 mg, 94%). $^1$H NMR (250 MHz, $CDCl_3$) δ 9.30 (s, 1H), 8.69 (s, 1H), 7.91 (s, 1H), 7.72−7.56 (m, 3H), 7.46−7.30 (m, 2H), 6.46 (s, 1H), 4.36 (q, $J$ = 7.25 Hz, 2H), 4.28−3.96 (m, 8H), 1.48 (t, $J$ = 7.04 Hz, 3H) ppm.

**2-(4-{[(2-Benzothiadiazolphenyl)amino]carbonothioyl}-1-piperazinyl)-8-ethyl-5-oxo-5,8-dihydropyrido[2,3-*d*]pyrimidine-6-carboxylic Acid (10).** Pipemidic acid (25 mg, 0.0824 mmol), 2,1,3-benzothiadiazol-4-yl isothiocyanate (16 mg, 0.0824 mmol), and triethylamine (23 μL, 0.165 mmol) were used. Purification on silica yielded **10** (10.8 mg, 26%). $^1$H NMR (300 MHz, DMSO) δ 9.81 (s, 1H), 9.27 (s, 1H), 9.00 (s, 1H), 7.93 (d, $J$ = 8.40 Hz, 1H), 7.77−7.68 (m, 1H), 7.63 (d, $J$ = 7.23 Hz, 1H), 4.48−4.41 (m, 2H), 4.24−3.99 (m, 8H), 1.39 (t, $J$ = 6.52 3H) ppm.

**2-(4-{[(3-Trifluoromethylphenyl)amino]carbonothioyl}-1-piperazinyl)-8-ethyl-5-oxo-5,8-dihydropyrido[2,3-*d*]pyrimidine-6-carboxylic Acid (11).** Pipemidic acid (25 mg, 0.0824 mmol), 3-(trifluoromethyl)phenyl isothiocyanate (12.5 μL, 0.0824 mmol), and triethylamine (23 μL, 0.165 mmol) were used. Purification on silica yielded **11** (31 mg, 75%). $^1$H NMR (300 MHz, $CDCl_3$) δ 9.32 (s, 1H), 8.72 (s, 1H), 7.41−7.35 (m, 1H), 7.29−7.21 (m, 2H), 7.21−7.16 (m, 1H), 4.37 (q, $J$ = 7.10 Hz, 2H), 4.27−3.93 (m, 8H), 1.50 (t, $J$ = 7.04 Hz, 3H) ppm.

**2-(4-{[(2-Trifluoromethylphenyl)amino]carbonothioyl}-1-piperazinyl)-8-ethyl-5-oxo-5,8-dihydropyrido[2,3-*d*]pyrimidine-6-carboxylic Acid (12).** Pipemidic acid (48 mg, 0.159 mmol) and 2-(trifluoromethyl)phenyl isothiocyanate (20 μL, 0.132 mmol) were used. Purification on silica yielded **12** (55 mg, 82%). $^1$H NMR (300 MHz, $CDCl_3$) δ 9.32 (s, 1H), 8.69 (s, 1H), 7.74−7.64 (m, 1H), 7.63−7.51 (m, 2H), 7.43−7.33 (m, 1H), 4.47−3.90 (m, 10H), 1.50 (t, $J$ = 6.86 Hz, 3H) ppm.

**2-(4-{[(3-Methylphenyl)amino]carbonothioyl}-1-piperazinyl)-8-ethyl-5-oxo-5,8-dihydropyrido[2,3-*d*]pyrimidine-6-carboxylic Acid (13).** Pipemidic acid (54 mg, 0.177 mmol) and *m*-tolylisothiocyanate (20 μL, 0.148 mmol) were used. Purification on silica yielded **13** (67 mg, 100%).$^1$H NMR (300 MHz, $CDCl_3$) δ 9.32 (s, 1H), 8.68 (s, 1H), 7.34−7.32 (m, 1H), 7.05−6.94 (m, 3H), 4.33 (q, $J$ = 7.10 Hz, 2H), 4.24−3.87 (m, 8H), 2.35 (s, 3H), 1.49 (t, $J$ = 7.19 Hz, 3H) ppm.

**2-(4-{[(3-Chlorophenyl)amino]carbonothioyl}-1-piperazinyl)-8-ethyl-5-oxo-5,8-dihydropyrido[2,3-*d*]pyrimidine-6-carboxylic Acid (14).** Pipemidic acid (25 mg, 0.0824 mmol), 3-chlorophenyl isothiocyanate (11 μL, 0.0824 mmol), and triethylamine (23 μL, 0.165 mmol) were used. Purification on silica yielded **14** (8.2 mg, 21%). $^1$H NMR (300 MHz, $CDCl_3$) δ 9.03 (s, 1H), 8.51 (s, 1H), 7.10 (s, 1H), 7.04−6.93 (m, 2H), 6.90−6.84 (m, 1H), 4.14 (q, $J$ = 6.90 Hz, 2H), 4.00−3.74 (m, 8H), 1.23 (t, $J$ = 7.01 Hz, 3H) ppm.

**2-(4-{[(2,3-Dichlorophenyl)amino]carbonothioyl}-1-piperazinyl)-8-ethyl-5-oxo-5,8-dihydropyrido[2,3-*d*]pyrimidine-6-carboxylic Acid (15).** Pipemidic acid (51 mg, 0.168 mmol) and 2,3-dichlorophenyl isothiocyanate (20 μL, 0.141 mmol) were used. Purification on silica yielded **15** (15.5 mg, 22%). $^1$H NMR (300 MHz, DMSO) δ 9.03 (s, 1H), 8.78 (s, 1H), 7.53 (d, $J$ = 7.43 Hz, 1H), 7.41−7.26 (m, 2H), 4.51−3.90 (m, 10H), 1.43−1.27 (m, 3H) ppm.

**2-(4-{[(Phenyl)amino]carbonothioyl}-1-piperazinyl)-8-ethyl-5-oxo-5,8-dihydropyrido[2,3-*d*]pyrimidine-6-carboxylic Acid phenyl (16).** Pipemidic acid (25 mg, 0.0824 mmol), phenyl isothiocyanate (9.8 μL, 0.0824 mmol), and triethylamine (23 μL, 0.165 mmol) were used. Purification on silica yielded **16** (16 mg, 43%). $^1$H NMR (300 MHz, $CDCl_3$) δ 9.33 (s, 1H), 8.68 (s, 1H), 7.41−7.33 (m, 3H), 7.22−7.15 (m, 2H), 4.38−4.28 (m, 2H), 4.24−3.89 (m, 8H), 1.49 (t, $J$ = 7.57 Hz, 3H) ppm.

**2-(4-{[(2-Chlorophenyl)amino]carbonothioyl}-1-piperazinyl)-8-ethyl-5-oxo-5,8-dihydropyrido[2,3-*d*]pyrimidine-6-carboxylic Acid (17).** Pipemidic acid (56 mg, 0.184 mmol) and 2-chlorophenylisothiocyanate (20 μL, 0.153 mmol) were used. Purification on silica yielded **17** (72 mg, 99%). $^1$H NMR (300 MHz, $CDCl_3$) δ 9.34 (s, 1H), 8.68 (s, 1H), 7.75 (d, $J$ = 8.10 Hz, 1H), 7.44 (d, $J$ = 8.00 Hz, 1H), 7.37−7.27 (m, 2H), 7.15 (t, $J$ = 7.67 Hz, 1H), 4.35 (q, $J$ = 7.15 Hz, 2H), 4.29−4.01 (m, 8H), 1.50 (t, $J$ = 7.20 Hz, 3H) ppm.

**2-(4-{[(3,5-Bis(trifluoromethyl)phenyl)amino]carbonothioyl}-1-piperazinyl)-8-ethyl-5-oxo-5,8-dihydropyrido[2,3-*d*]pyrimidine-6-carboxylic Acid (18).** Pipemidic acid (40 mg, 0.132 mmol) and 3,5-bis(trifluoromethyl)phenyl isothiocyanate (20 μL, 0.110 mmol) were used. Purification on silica yielded **18** (61 mg, 97%). $^1$H NMR (300 MHz, $CDCl_3$) δ 9.30 (s, 1H), 8.68 (s, 1H), 8.62 (s, 1H), 7.94 (s, 2H), 7.62 (s, 1H), 4.42−4.05 (m, 10H), 1.51 (t, $J$ = 7.07 Hz, 3H) ppm.

**2-(4-{[(3-Methoxyphenyl)amino]carbonothioyl}-1-piperazinyl)-8-ethyl-5-oxo-5,8-dihydropyrido[2,3-*d*]pyrimidine-6-carboxylic Acid (19).** Pipemidic acid (25 mg, 0.0824 mmol), 3-methoxyphenyl isothiocyanate (11.6 μL, 0.0824 mmol), and triethylamine (23 μL, 0.165 mmol) were used. Purification on silica yielded **19** (21.4 mg, 55%). $^1$H NMR (300 MHz, $CDCl_3$) δ 9.31 (s, 1H), 8.67 (s, 1H), 7.47 (s, 1H), 7.30−7.21 (m, 1H), 6.80−6.68 (m, 3H), 4.32 (q, $J$ = 6.90 Hz, 2H), 4.23−3.89 (m, 8H), 3.79 (s, 3H), 1.48 (t, $J$ = 7.16 Hz, 3H) ppm.

**2-(4-{[(2,5-Dichlorophenyl)amino]carbonothioyl}-1-piperazinyl)-8-ethyl-5-oxo-5,8-dihydropyrido[2,3-*d*]pyrimidine-6-carboxylic Acid (20).** Pipemidic acid (51 mg, 0.168 mmol) and 2,5-dichlorophenyl isothiocyanate (20 μL, 0.140 mmol) were used. Purification on silica yielded **20** (42.7 mg, 60%). $^1$H NMR (300 MHz, $CDCl_3$) δ 9.39 (s, 1H), 9.06 (s, 1H), 7.57 (d, $J$ = 2.39 Hz, 1H), 7.42−7.36 (m, 1H), 7.20 (d, $J$ = 7.35 Hz, 1H), 4.55−4.39 (m, 2H), 4.31−4.02 (m, 8H), 1.52 (t, $J$ = 6.88 Hz, 3H) ppm.

**2-(4-{[(2-Methoxyphenyl)amino]carbonothioyl}-1-piperazinyl)-8-ethyl-5-oxo-5,8-dihydropyrido[2,3-*d*]pyrimidine-6-carboxylic Acid (21).** Pipemidic acid (53 mg, 0.175 mmol) and 2-methoxyphenyl isothiocyanate (20 μL, 0.145 mmol) were used. Purification on silica yielded **21** (36 mg, 53%). $^1$H NMR (250 MHz, $CDCl_3$) δ 9.33 (s, 1H), 8.68 (s, 1H), 7.84 (d, $J$ = 7.30 Hz, 1H), 7.54 (s, 1H), 7.20−7.04 (m, 1H), 7.03−6.85 (m, 2H), 4.44−3.73 (m, 13H), 1.49 (t, $J$ = 6.60 Hz, 3H) ppm.

**2-(4-{[(3,5-Dimethylphenyl)amino]carbonothioyl}-1-piperazinyl)-8-ethyl-5-oxo-5,8-dihydropyrido[2,3-*d*]pyrimidine-6-carboxylic Acid (22).** Pipemidic acid (45 mg, 0.148 mmol), 3,5-dimethylphenyl isothiocyanate (24 mg, 0.148 mmol), and triethylamine (41 μL, 0.296 mmol) were used. Purification on silica yielded **22** (41.6 mg, 67%). $^1$H NMR (300 MHz, $CDCl_3$) δ 9.30 (s, 1H), 8.66 (s, 1H), 7.48 (s, 1H), 6.86−6.75 (m, 3H), 4.33 (q, $J$ = 7.10 Hz, 2H), 4.22−3.91 (m, 8H), 2.30 (s, 6H), 1.48 (t, $J$ = 7.11 Hz, 3H) ppm.

**2-(4-{[(4-Fluorophenyl)amino]carbonothioyl}-1-piperazinyl)-8-ethyl-5-oxo-5,8-dihydropyrido[2,3-*d*]pyrimidine-6-carboxylic Acid (23).** Pipemidic acid (35 mg, 0.1154 mmol) and 4-fluorophenyl isothiocyanate (17.7 mg, 0.1154 mmol) were used. Purification on silica yielded **23** (30 mg, 57%). $^1$H NMR (300 MHz, $CDCl_3$) δ 9.34 (s, 1H), 8.69 (s, 1H), 7.33 (s, 1H), 7.25−7.16 (m, 2H), 7.13−7.03 (m, 2H), 4.34 (q, $J$ = 7.00 Hz, 2H), 4.28−3.96 (m, 8H), 1.50 (t, $J$ = 7.36 Hz, 3H) ppm.

**2-(4-{[(4-Methoxyphenyl)amino]carbonothioyl}-1-piperazinyl)-8-ethyl-5-oxo-5,8-dihydropyrido[2,3-*d*]pyrimidine-6-carboxylic Acid (24).** Pipemidic acid (30 mg, 0.0989 mmol) and 4-methoxyphenyl isothiocyanate (13.7 μL, 0.0989 mmol) were used.

Purification on silica yielded **24** (37 mg, 80%). $^1$H NMR (300 MHz, $CDCl_3$) $\delta$ 9.33 (s, 1H), 8.67 (s, 1H), 7.30 (s, 1H), 7.15 (d, $J$ = 8.76 Hz, 2H), 6.90 (d, $J$ = 8.82 Hz, 2H), 4.34 (q, $J$ = 7.10 Hz, 2H), 4.25−3.92 (m, 8H), 3.81 (s, 3H), 1.49 (t, $J$ = 7.12 Hz, 3H) ppm.

**2-(4-{[(3-Fluorophenyl)amino]carbonothioyl}-1-piperazinyl)-8-ethyl-5-oxo-5,8-dihydropyrido[2,3-*d*]pyrimidine-6-carboxylic Acid (25).** Pipemidic acid (25 mg, 0.0824 mmol) and 3-fluorophenyl isothiocyanate (9.9 $\mu$L, 0.0824 mmol) were used. Purification on silica yielded **25** (22 mg, 59%). $^1$H NMR (300 MHz, $CDCl_3$) $\delta$ 9.32 (s, 1H), 8.66 (s, 1H), 7.41 (s, 1H), 7.37−7.27 (m, 1H), 6.96 (t, $J$ = 7.39, 2H), 6.88 (t, $J$ = 7.67 Hz, 1H), 4.38−4.27 (m, 2H), 4.27−3.91 (m, 8H), 1.54−1.43 (m, 3H) ppm.

**2-(4-{[(2-Iodophenyl)amino]carbonothioyl}-1-piperazinyl)-8-ethyl-5-oxo-5,8-dihydropyrido[2,3-*d*]pyrimidine-6-carboxylic Acid (26).** Pipemidic acid (25 mg, 0.0824 mmol) and 2-iodophenyl isothiocyanate (21.5 mg, 0.0824 mmol) were used. Purification on silica yielded **26** (35 mg, 75%). $^1$H NMR (300 MHz, $CDCl_3$) $\delta$ 9.36−9.30 (m, 1H), 8.69−8.65 (m, 1H), 7.89−7.82 (m, 1H), 7.62−7.55 (m, 1H), 7.41−7.32 (m, 1H), 7.00−6.92 (m, 1H), 4.40−4.01 (m, 10H), 1.53−1.44 (m, 3H) ppm.

**2-(4-{[(4-Methylphenyl)amino]carbonothioyl}-1-piperazinyl)-8-ethyl-5-oxo-5,8-dihydropyrido[2,3-*d*]pyrimidine-6-carboxylic Acid (27).** Pipemidic acid (89 mg, 0.293 mmol) and *p*-tolyl isothiocyanate (40 mg, 0.268 mmol) were used. Purification on silica yielded **27** (82 mg, 68%). $^1$H NMR (300 MHz, $CDCl_3$) $\delta$ 9.32 (s, 1H), 8.67 (s, 1H), 7.40 (s, 1H), 7.17 (d, $J$ = 7.60 Hz, 2H), 7.09 (d, $J$ = 7.44 Hz, 2H), 4.33 (q, $J$ = 6.40 Hz, 2H), 4.23−3.91 (m, 8H), 2.34 (s, 3H), 1.49 (t, $J$ = 7.03 Hz, 3H) ppm.

**2-(4-{[(4-Chlorophenyl)amino]carbonothioyl}-1-piperazinyl)-8-ethyl-5-oxo-5,8-dihydropyrido[2,3-*d*]pyrimidine-6-carboxylic Acid (28).** Pipemidic acid (58 mg, 0.191 mmol) and 4-chlorophenyl isothiocyanate (27 mg, 0.159 mmol) were used. Purification on silica yielded **28** (50 mg, 67%). $^1$H NMR (300 MHz, $CDCl_3$) $\delta$ 9.34 (s, 1H), 8.68 (s, 1H), 7.36−7.34 (m, 2H), 7.17 (d, $J$ = 8.70 Hz, 2H), 4.39−4.28 (m, 2H), 4.28−3.93 (m, 8H), 1.49 (t, $J$ = 6.68 Hz, 3H) ppm.

**2-(4-{[(3-Iodophenyl)amino]carbonothioyl}-1-piperazinyl)-8-ethyl-5-oxo-5,8-dihydropyrido[2,3-*d*]pyrimidine-6-carboxylic Acid (29).** Pipemidic acid (40 mg, 0.133 mmol) and 3-iodophenyl isothiocyanate (29 mg, 0.111 mmol) were used. Purification on silica yielded **29** (57 mg, 90%). $^1$H NMR (250 MHz, $CDCl_3$) $\delta$ 9.33 (s, 1H), 8.73 (s, 1H), 7.66−7.64 (m, 1H), 7.54−7.51 (m, 1H), 7.40−7.24 (m, 1H), 7.12−7.06 (m, 1H), 4.48−4.31 (m, 2H), 4.27−3.93 (m, 8H), 1.34−1.17 (m, 3H) ppm.

**2-(4-{[(2-Fluorophenyl)amino]carbonothioyl}-1-piperazinyl)-8-ethyl-5-oxo-5,8-dihydropyrido[2,3-*d*]pyrimidine-6-carboxylic Acid (30).** Pipemidic acid (25 mg, 0.0824 mmol) and 2-fluorophenyl isothiocyanate (10 $\mu$L, 0.0824 mmol) were used. Purification on silica yielded **30** (24 mg, 64%). $^1$H NMR (300 MHz, $CDCl_3$) $\delta$ 9.35 (s, 1H), 8.69 (s, 1H), 7.64 (t, $J$ = 7.34 Hz, 1H), 7.21−7.12 (m, 3H), 4.35 (q, $J$ = 6.90 Hz, 2H), 4.28−4.02 (m, 8H), 1.50 (t, $J$ = 7.09 Hz, 3H) ppm.

**2-(4-{[(4-Trifluoromethylphenyl)amino]carbonothioyl}-1-piperazinyl)-8-ethyl-5-oxo-5,8-dihydropyrido[2,3-*d*]pyrimidine-6-carboxylic Acid (31).** Pipemidic acid (30 mg, 0.0989 mmol) and 4-trifluoromethylphenyl isothiocyanate (16.7 mg, 0.0824 mmol) were used. Purification on silica yielded **31** (31 mg, 77%). $^1$H NMR (300 MHz, $CDCl_3$) $\delta$ 9.34 (s, 1H), 8.69 (s, 1H), 7.65−7.57 (m, 2H), 7.51 (s, 1H), 7.37−7.31 (m, 2H), 4.34 (q, $J$ = 6.80 Hz, 2H), 4.27−3.97 (m, 8H), 1.49 (t, $J$ = 7.25, 7.25 Hz, 3H) ppm.

**Acknowledgment.** The authors are grateful to the Chemical Computing Group for free access to the Molecular Operating Environment (MOE) software. This work was supported, in part, by a research grant from the Elsa U. Pardee Foundation (A.L.P. and D.L.B.).

**Supporting Information Available:** Proposed ATX analogs for lead optimization and NPP6 and NPP7 selectivity results. This material is available free of charge via the Internet at http://pubs.acs.org.

## References

(1) Stracke, M. L.; Krutzsch, H. C.; Unsworth, E. J.; Årestad, A.; Cioce, V.; Schiffmann, E.; Liotta, L. A. Identification, purification, and partial sequence analysis of autotaxin, a novel motility-stimulating protein. *J. Biol. Chem.* **1992**, *267*, 2524–2529.

(2) Umezu-Goto, M.; Kishi, Y.; Taira, A.; Hama, K.; Dohmae, N.; Takio, K.; Yamori, T.; Mills, G. B.; Inoue, K.; Aoki, J.; Arai, H. Autotaxin has lysophospholipase D activity leading to tumor cell growth and motility by lysophosphatidic acid production. *J. Cell Biol.* **2002**, *158*, 227–233.

(3) Tokumura, A.; Majima, E.; Kariya, Y.; Tominaga, K.; Kogure, K.; Yasuda, K.; Fukuzawa, K. Identification of human plasma lysophospholipase D, a lysophosphatidic acid-producing enzyme, as autotaxin, a multifunctional phosphodiesterase. *J. Biol. Chem.* **2002**, *277*, 39436–39442.

(4) Tanaka, M.; Okudaira, S.; Kishi, Y.; Ohkawa, R.; Iseki, S.; Ota, M.; Noji, S.; Yatomi, Y.; Aoki, J.; Arai, H. Autotaxin stabilizes blood vessels and is required for embryonic vasculature by producing lysophosphatidic acid. *J. Biol. Chem.* **2006**, *281*, 25822–25830.

(5) Singer, S. J.; Kupfer, A. The directed migration of eukaryotic cells. *Annu. Rev. Cell Biol.* **1986**, *2*, 337–365.

(6) van Meeteren, L. A.; Ruurs, P.; Stortelers, C.; Bouwman, P.; van Rooijen, M. A.; Pradere, J. P.; Pettit, T. R.; Wakelam, M. J.; Saulnier-Blache, J. S.; Mummery, C. L.; Moolenaar, W. H.; Jonkers, J. Autotaxin, a secreted lysophospholipase D, is essential for blood vessel formation during development. *Mol. Cell. Biol.* **2006**, *26*, 5015–5022.

(7) Tokumura, A.; Kanaya, Y.; Miyake, M.; Yamano, S.; Irahara, M.; Fukuzawa, K. Increased production of bioactive lysophosphatidic acid by serum lysophospholipase D in human pregnancy. *Biol. Reprod.* **2002**, *67*, 1386–1392.

(8) Baumforth, K. R.; Flavell, J. R.; Reynolds, G. M.; Davies, G.; Pettit, T. R.; Wei, W.; Morgan, S.; Stankovic, T.; Kishi, Y.; Arai, H.; Nowakova, M.; Pratt, G.; Aoki, J.; Wakelam, M. J.; Young, L. S.; Murray, P. G. Induction of autotaxin by the Epstein-Barr virus promotes the growth and survival of Hodgkin lymphoma cells. *Blood* **2005**, *106*, 2138–2146.

(9) Chen, M.; O'Connor, K. L. Integrin alpha6beta4 promotes expression of autotaxin/ENPP2 autocrine motility factor in breast carcinoma cells. *Oncogene* **2005**, *24*, 5125–5130.

(10) Euer, N.; Schwirzke, M.; Evtimova, V.; Burtscher, H.; Jarsch, M.; Tarin, D.; Weidle, U. H. Identification of genes associated with metastasis of mammary carcinoma in metastatic versus non-metastatic cell lines. *Anticancer Res.* **2002**, *22*, 733–740.

(11) Hoelzinger, D. B.; Mariani, L.; Weis, J.; Woyke, T.; Berens, T. J.; McDonough, W. S.; Sloan, A.; Coons, S. W.; Berens, M. E. Gene expression profile of glioblastoma multiforme invasive phenotype points to new therapeutic targets. *Neoplasia* **2005**, *7*, 7–16.

(12) Kawagoe, H.; Stracke, M. L.; Nakamura, H.; Sano, K. Expression and transcriptional regulation of the PD-Ialpha/autotaxin gene in neuroblastoma. *Cancer Res.* **1997**, *57*, 2516–2521.

(13) Kehlen, A.; Englert, N.; Seifert, A.; Klonisch, T.; Dralle, H.; Langner, J.; Hoang-Vu, C. Expression, regulation and function of autotaxin in thyroid carcinomas. *Int. J. Cancer* **2004**, *109*, 833–838.

(14) Koh, E.; Bandle, R. W.; Roberts, D. D.; Stracke, M. L.; Clair, T. Novel point mutations attenuate autotaxin activity. *Lipids Health Dis.* **2009**, *8*, 4.

(15) Lee, H. Y.; Murata, J.; Clair, T.; Polymeropoulos, M. H.; Torres, R.; Manrow, R. E.; Liotta, L. A.; Stracke, M. L. Cloning, chromosomal localization, and tissue expression of autotaxin from human teratocarcinoma cells. *Biochem. Biophys. Res. Commun.* **1996**, *218*, 714–719.

(16) Masuda, A.; Nakamura, K.; Izutsu, K.; Igarashi, K.; Ohkawa, R.; Jona, M.; Higashi, K.; Yokota, H.; Okudaira, S.; Kishimoto, T.; Watanabe, T.; Koike, Y.; Ikeda, H.; Kozai, Y.; Kurokawa, M.; Aoki, J.; Yatomi, Y. Serum autotaxin measurement in haematological malignancies: A promising marker for follicular lymphoma. *Br. J. Hamaetol.* **2008**, *143*, 60–70.

(17) Song, J.; Clair, T.; Noh, J. H.; Eun, J. W.; Ryu, S. Y.; Lee, S. N.; Ahn, Y. M.; Kim, S. Y.; Lee, S. H.; Park, W. S.; Yoo, N. J.; Lee, J. Y.; Nam, S. W. Autotaxin (lysoPLD/NPP2) protects fibroblasts from apoptosis through its enzymatic product, lysophosphatidic acid, utilizing albumin-bound substrate. *Biochem. Biophys. Res. Commun.* **2005**, *337*, 967–975.

(18) Stassar, M. J.; Devitt, G.; Brosius, M.; Rinnab, L.; Prang, J.; Schradin, T.; Simon, J.; Petersen, S.; Kopp-Schneider, A.; Zoller, M. Identification of human renal cell carcinoma associated genes by suppression subtractive hybridization. *Br. J. Cancer* **2001**, *85*, 1372–1382.
(19) Zeng, Y.; Kakehi, Y.; Nouh, M. A.; Tsunemori, H.; Sugimoto, M.; Wu, X. X. Gene expression profiles of lysophosphatidic acid-related molecules in the prostate: relevance to prostate cancer and benign hyperplasia. *Prostate* **2009**, *69*, 283–292.
(20) Zhang, G.; Zhao, Z.; Xu, S.; Ni, L.; Wang, X. Expression of autotaxin mRNA in human hepatocellular carcinoma. *Chin. Med. J. (Engl.)* **1999**, *112*, 330–332.
(21) Hammack, B. N.; Fung, K. Y.; Hunsucker, S. W.; Duncan, M. W.; Burgoon, M. P.; Owens, G. P.; Gilden, D. H. Proteomic analysis of multiple sclerosis cerebrospinal fluid. *Mult. Scler.* **2004**, *10*, 245–260.
(22) Boucher, J.; Quilliot, D.; Praderes, J. P.; Simon, M. F.; Gres, S.; Guigne, C.; Prevot, D.; Ferry, G.; Boutin, J. A.; Carpene, C.; Valet, P.; Saulnier-Blache, J. S. Potential involvement of adipocyte insulin resistance in obesity-associated up-regulation of adipocyte lysophospholipase D/autotaxin expression. *Diabetologia* **2005**, *48*, 569–577.
(23) Ferry, G.; Tellier, E.; Try, A.; Grés, S.; Naime, I.; Simon, M. F.; Rodriguez, M.; Boucher, J.; Tack, I.; Gesta, S.; Chomarat, P.; Dieu, M.; Raes, M.; Galizzi, J. P.; Valet, P.; Boutin, J. A.; Saulnier-Blache, J. S. Autotaxin is released from adipocytes, catalyzes lysophosphatidic acid synthesis, and activates preadipocyte proliferation. *J. Biol. Chem.* **2003**, *278*, 18162–18169.
(24) Gesta, S.; Simon, M. F.; Rey, A.; Sibrac, D.; Girard, A.; Lafontan, M.; Valet, P.; Saulnier-Blache, J. S. Secretion of a lysophospholipase D activity by adipocytes: involvement in lysophosphatidic acid synthesis. *J. Lipid Res.* **2002**, *43*, 904–910.
(25) Simon, M. F.; Daviaud, D.; Pradere, J. P.; Gres, S.; Guigne, C.; Wabitsch, M.; Chun, J.; Valet, P.; Saulnier-Blache, J. S. Lysophosphatidic acid inhibits adipocyte differentiation via lysophosphatidic acid 1 receptor-dependent down-regulation of peroxisome proliferator-activated receptor gamma2. *J. Biol. Chem.* **2005**, *280*, 14656–14662.
(26) Simon, M. F.; Rey, A.; Castan-Laurel, I.; Gres, S.; Sibrac, D.; Valet, P.; Saulnier-Blache, J. S. Expression of ectolipid phosphate phosphohydrolases in 3T3F442A preadipocytes and adipocytes. Involvement in the control of lysophosphatidic acid production. *J. Biol. Chem.* **2002**, *277*, 23131–23136.
(27) Umemura, K.; Yamashita, N.; Yu, X.; Arima, K.; Asada, T.; Makifuchi, T.; Murayama, S.; Saito, Y.; Kanamaru, K.; Goto, Y.; Kohsaka, S.; Kanazawa, I.; Kimura, H. Autotaxin expression is enhanced in frontal cortex of Alzheimer-type dementia patients. *Neurosci. Lett.* **2006**, *400*, 97–100.
(28) Inoue, M.; Ma, L.; Aoki, J.; Chun, J.; Ueda, H. Autotaxin, a synthetic enzyme of lysophosphatidic acid (LPA), mediates the induction of nerve-injured neuropathic pain. *Mol. Pain* **2008**, *4*, 6.
(29) Inoue, M.; Ma, L.; Aoki, J.; Ueda, H. Simultaneous stimulation of spinal NK1 and NMDA receptors produces LPC which undergoes ATX-mediated conversion to LPA, an initiator of neuropathic pain. *J. Neurochem.* **2008**, *107*, 1556–1565.
(30) Inoue, M.; Xie, W.; Matsushita, Y.; Chun, J.; Aoki, J.; Ueda, H. Lysophosphatidylcholine induces neuropathic pain through an action of autotaxin to generate lysophosphatidic acid. *Neuroscience* **2008**, *152*, 296–298.
(31) Tokumura, A.; Miyake, M.; Yoshimoto, O.; Shimizu, M.; Fukuzawa, K. Metal-ion stimulation and inhibition of lysophospholipase D which generates bioactive lysophosphatidic acid in rat plasma. *Lipids* **1998**, *33*, 1009–1015.
(32) Clair, T.; Koh, E.; Ptaszynska, M.; Bandle, R. W.; Liotta, L. A.; Schiffmann, E.; Stracke, M. L. L-histidine inhibits production of lysophosphatidic acid by the tumor-associated cytokine, autotaxin. *Lipids Health Dis.* **2005**, *4*, 5.
(33) van Meeteren, L. A.; Ruurs, P.; Christodoulou, E.; Goding, J. W.; Takakusa, H.; Kikuchi, K.; Perrakis, A.; Nagano, T.; Moolenaar, W. H. Inhibition of autotaxin by lysophosphatidic acid and sphingosine 1-phosphate. *J. Biol. Chem.* **2005**, *280*, 21155–21161.
(34) Durgam, G. G.; Virag, T.; Walker, M. D.; Tsukahara, R.; Yasuda, S.; Liliom, K.; van Meeteren, L. A.; Moolenaar, W. H.; Wilke, N.; Siess, W.; Tigyi, G.; Miller, D. D. Synthesis, structure-activity relationships, and biological evaluation of fatty alcohol phosphates as lysophosphatidic acid receptor ligands, activators of PPARgamma, and inhibitors of autotaxin. *J. Med. Chem.* **2005**, *48*, 4919–4930.
(35) Gududuru, V.; Zeng, K.; Tsukahara, R.; Makarova, N.; Fujiwara, Y.; Pigg, K. R.; Baker, D. L.; Tigyi, G.; Miller, D. D. Identification of Darmstoff analogs as selective agonists and antagonists of lysophosphatidic acid receptors. *Bioorg. Med. Chem. Lett.* **2006**, *16*, 451–456.
(36) Baker, D. L.; Fujiwara, Y.; Pigg, K. R.; Tsukahara, R.; Kobayashi, S.; Murofushi, H.; Uchiyama, A.; Murakami-Murofushi, K.; Koh, E.; Bandle, R. W.; Byun, H.-S.; Bittman, R.; Fan, D.; Murph, M.; Mills, G. B.; Tigyi, G. Carba analogs of cyclic phosphatidic acid are selective inhibitors of autotaxin and cancer cell invasion and metastasis. *J. Biol. Chem.* **2005**, *281*, 22786–22793.
(37) Cui, P.; Tonsig, J. L.; McCalmont, W. F.; Lee, S.; Becker, C. J.; Lynch, K. R.; Macdonald, T. L. Synthesis and biological evaluation of phosphonate derivatives as autotaxin (ATX) inhibitors. *Bioorg. Med. Chem. Lett.* **2007**, *17*, 1634–1640.
(38) Ferry, G.; Moulharat, N.; Pradere, J. P.; Desos, P.; Try, A.; Genton, A.; Giganti, A.; Beucher-Gaudin, M.; Lonchampt, M.; Bertrand, M.; Saulnier-Blache, J. S.; Tucker, G. C.; Cordi, A.; Boutin, J. A. S32826, a nanomolar inhibitor of autotaxin: discovery, synthesis and applications as a pharmacological tool. *J. Pharmacol. Exp. Ther.* **2008**, *327*, 809–819.
(39) Prestwich, G. D.; Gajewiak, J.; Zhang, H.; Xu, X.; Yang, G.; Serban, M. Phosphatase-resistant analogues of lysophosphatidic acid: Agonists promote healing, antagonists and autotaxin inhibitors treat cancer. *Biochim. Biophys. Acta* **2008**, *1781*, 588–594.
(40) van Meeteren, L. A.; Brinkmann, V.; Saulnier-Blache, J. S.; Lynch, K. R.; Moolenaar, W. H. Anticancer activity of FTY720: Phosphorylated FTY720 inhibits autotaxin, a metastasis-enhancing and angiogenic lysophospholipase D. *Cancer Lett.* **2008**, *266*, 203–208.
(41) Lipinski, C. A.; Lombardo, F.; Dominy, B. W.; Feeney, P. J. Experimental and computational approaches to estimate solubility and permeability in drug discovery and development settings. *Adv. Drug Delivery Rev.* **2001**, *46*, 3–26.
(42) Keller, T. H.; Pichota, A.; Yin, Z. A practical view of 'druggability'. *Curr. Opin. Chem. Biol.* **2006**, *10*, 357–361.
(43) Parrill, A. L.; Echols, U.; Nguyen, T.; Pham, T. C.; Hoeglund, A.; Baker, D. L. Virtual screening approaches for the identification of non-lipid autotaxin inhibitors. *Bioorg. Med. Chem.* **2008**, *16*, 1784–1795.
(44) Saunders, L. P.; Ouellette, A.; Bandle, R.; Chang, W. C.; Zhou, H.; Misra, R. N.; De La Cruz, E. M.; Braddock, D. T. Identification of small-molecule inhibitors of autotaxin that inhibit melanoma cell migration and invasion. *Mol. Cancer Ther.* **2008**, *7*, 3352–3362.
(45) Ferguson, C. G.; Bigman, C. S.; Richardson, R. D.; van Meeteren, L. A.; Moolenaar, W. H.; Prestwich, G. D. Fluorogenic phospholipid substrate to detect lysophospholipase D/autotaxin activity. *Org. Lett.* **2006**, *8*, 2023–2026.
(46) Moulharat, N.; Fould, B.; Giganti, A.; Boutin, J. A.; Ferry, G. Molecular pharmacology of adipocyte-secreted autotaxin. *Chem.-Biol. Interact.* **2008**, *172*, 115–124.
(47) Stefan, C.; Jansen, S.; Bollen, M. NPP-type ectophosphodiesterases: unity in diversity. *Trends Biochem. Sci.* **2005**, *30*, 542–550.
(48) Lee, M. J.; Van Brocklyn, J. R.; Thangada, S.; Liu, C. H.; Hand, A. R.; Menzeleev, R.; Spiegel, S.; Hla, T. Sphingosine-1-phosphate as a ligand for the G protein-coupled receptor EDG-1. *Science* **1998**, *279*, 1552–1555.
(49) Sakagami, H.; Aoki, J.; Natori, Y.; Nishikawa, K.; Kakehi, Y.; Natori, Y.; Arai, H. Biochemical and molecular characterization of a novel choline-specific glycerophosphodiester phosphodiesterase belonging to the nucleotide pyrophosphatase/phosphodiesterase family. *J. Biol. Chem.* **2005**, *280*, 23084–23093.
(50) Duan, R. D.; Bergman, T.; Xu, N.; Wu, J.; Cheng, Y.; Duan, J.; Nelander, S.; Palmberg, C.; Nilsson, A. Identification of human intestinal alkaline sphingomyelinase as a novel ecto-enzyme related to the nucleotide phosphodiesterase family. *J. Biol. Chem.* **2003**, *278*, 38528–38536.
(51) Duan, R. D.; Cheng, Y.; Hansen, G.; Hertervig, E.; Liu, J. J.; Syk, I.; Sjostrom, H.; Nilsson, A. Purification, localization, and expression of human intestinal alkaline sphingomyelinase. *J. Lipid Res.* **2003**, *44*, 1241–1250.
(52) Wu, J.; Nilsson, A.; Jonsson, B. A.; Stenstad, H.; Agace, W.; Cheng, Y.; Duan, R. D. Intestinal alkaline sphingomyelinase hydrolyses and inactivates platelet-activating factor by a phospholipase C activity. *Biochem. J.* **2006**, *394*, 299–308.
(53) Wu, J.; Hansen, G. H.; Nilsson, A.; Duan, R. D. Functional studies of human intestinal alkaline sphingomyelinase by deglycosylation and mutagenesis. *Biochem. J.* **2005**, *386*, 153–160.
(54) Cui, P.; McCalmont, W. F.; Tomsig, J. L.; Lynch, K. R.; Macdonald, T. L. alpha- and beta-substituted phosphonate analogs of LPA as autotaxin inhibitors. *Bioorg. Med. Chem.* **2008**, *16*, 2212–2225.
(55) Jiang, G.; Xu, Y.; Fujiwara, Y.; Tsukahara, T.; Tsukahara, R.; Gajewiak, J.; Tigyi, G.; Prestwich, G. D. α−substituted phosphonate analogues of lysophosphatidic acid (LPA) selectively inhibit production and action of LPA. *ChemMedChem* **2007**, *2*, 679–690.